

Molecular gas properties in young stellar clusters with a suppressed star cluster wind

SERGIY SILICH,¹ JEAN TURNER,² JONATHAN MACKEY,³ AND SERGIO MARTÍNEZ-GONZÁLEZ⁴

¹*Instituto Nacional de Astrofísica Óptica y Electrónica, AP 51, 72000, Puebla, México
email: silich@inaoep.mx*

²*UCLA Department of Physics and Astronomy, CA 90095-1547, Los Angeles, USA*

³*Dublin Institute for Advanced Studies, Astronomy & Astrophysics Section, DIAS Dunsink Observatory, Dublin
D15 XR2R, Ireland*

⁴*Instituto Nacional de Astrofísica Óptica y Electrónica, AP 51, 72000, Puebla, México*

(Dated: Accepted . Received ; in original form)

ABSTRACT

In compact and dense star-forming clouds a global star cluster wind could be suppressed. In this case the stellar feedback is unable to expel the leftover gas from the cluster. Young massive stars remain embedded into a dense residual gas and stir it moving in the gravitational well of the system. Here we present a self-consistent model for the molecular gas distribution in such young, enshrouded stellar clusters. It is assumed that the cloud collapse terminates and the star formation ceases when a balance between the turbulent pressure and gravity and between the turbulent energy dissipation and regeneration rates is established. These conditions result in an equation that determines the residual gas density distribution that, in turn, allows one to determine the other characteristics of the leftover gas and the star formation efficiency. It is shown that model predictions are in good agreement with several observationally determined properties of cloud D1 in nearby dwarf spheroidal galaxy NGC 5253 and its embedded cluster.

Keywords: galaxies: star formation — star clusters — individual (NGC 5253) — Physical Data and Processes: hydrodynamics

1. INTRODUCTION

Star formation is a fundamental problem in astrophysics for many years. There is a general agreement that star formation requires the dense molecular gas and occurs in giant molecular clouds. It was shown long time ago that the interstellar gas depletion time in our Galaxy is much longer than the free-fall time of molecular clouds (e.g. Williams & McKee 1997) that raised the problem of the molecular cloud stability and apparently low average star formation efficiency in our and other galaxies. Different solutions to these problems have been proposed and include strong magnetic fields (e.g. Shu et al. 1987), photoionization of the intracloud gas (McKee 1989; Franco et al. 1994) and different modifications of the feedback scenario - the injection of energy and momentum into the residual molecular gas by low-mass (Norman & Silk 1980; McKee 1989) or high-mass (Matzner 2002) stars (see a review by Padoan et al. 2014).

In contrast, to form a bound stellar cluster a large ($> 30\%$) star formation efficiency is required (Baumgardt & Kroupa 2007; Baumgardt et al. 2008). This raises the question how to prevent or at least retard the leftover gas expulsion and the molecular cloud disruption at early stages of massive star cluster formation (e.g. Wirth et al. (2022) claimed that it took 3.5Myr to 4.0Myr to stop star formation in Galactic globular clusters).

The supersonic velocity dispersion has been detected in objects of different scales from cores of molecular clouds and compact, young, still enshrouded by molecular gas stellar clusters, to giant HII regions and HII galaxies. This led Terlevich & Melnick (1981), Solomon et al. (1987) and Melnick et al. (1987) to suggest that supersonic turbulence is a characteristic of the gas virial equilibrium and that the dynamic feedback from the newborn stars prevents the parental cloud from the further collapse.

Tenorio-Tagle et al. (1993) associated supersonic velocities with a collection of bow shocks around pre-main-sequence stars moving in the gravitational well of the cluster and suggested that these bow shocks stir and maintain supersonic turbulence until massive stars and supernovae expel the remaining gas from the cluster. However, the supersonic turbulence decays very rapidly (Stone et al. 1998; Mac Low 1999) that requires sources more powerful than low-mass stars to maintain supersonic turbulence in star-forming clouds (e.g. Murray et al. 2010). Different aspects of the supersonic turbulence in molecular clouds were reviewed by, among others, Scalo (1987), Vazquez-Semadeni et al. (2000), Elmegreen & Scalo (2004), Mac Low & Klessen (2004), McKee & Ostriker (2007), Padoan et al. (2014). Bow shocks, their turbulent mixing layers and wakes were also discussed by many authors (see Arthur & Hoare 2006; Wareing et al. 2007; Binette et al. 2009; Mackey et al. 2013, 2015; Henney & Arthur 2019, and references therein).

The role of massive stars in the turbulent energy regeneration was discussed by Matzner (2002) who considered HII regions as the major mechanism for the turbulent energy regeneration, but did not discuss the effects of the intracluster gas distribution.

Marks & Kroupa (2012) found that initial star cluster half-mass radii weakly depend on stellar mass (see their equation 7) and even for $10^5 - 10^6 M_\odot$ clusters hardly exceed 1pc. In such compact and massive star-forming regions wind-driven bubbles around individual massive stars stall before merging with their neighbors (see Silich & Tenorio-Tagle 2017, 2018) and ionizing photons are effectively absorbed by dust grains which re-emit them in the infrared waveband. Upon such conditions massive stars are not able to photoionize the bulk of leftover gas, form a global star cluster wind and expel the residual gas from the star-forming region. The negative stellar feedback is then suppressed. Instead, ultracompact HII regions (UCHII) embedded into the residual molecular gas are formed (Silich et al. 2020). However, Silich & Tenorio-Tagle (2017, 2018) considered only the mechanical equilibrium in star-forming clouds with an arbitrary selected star formation efficiency (SFE) and did not account for the rapid turbulent energy dissipation.

Here, following Norman & Silk (1980); McKee (1989); Matzner (2002) we assume that the pre-stellar cloud collapse is followed by a vigorous star formation that terminates when a balance between the turbulent pressure and gravity, and the turbulent energy dissipation and regeneration rates is established. In contrast with other authors (e.g. Padoan 1995; Krumholz & McKee 2005; Krumholz et al. 2006; Padoan & Nordlund 2011), we do not consider how star formation proceeds in the collapsing cloud, but assume that it results in a stellar cluster with a certain mass and a known stellar density distribution and that the further star formation is altered by the stellar feedback. It is also postulated that the cluster is sufficiently compact and dense to prevent the leftover gas expulsion, the post-star-forming system is dynamically stable and that stellar feedback compensates the turbulent energy dissipation continuously. Our aim is to find out how the leftover molecular gas is distributed and obtain its other characteristics upon such conditions. We show that the equilibrium conditions together with the only one free parameter that characterises the degree to which the feedback energy could be conserved, fix the residual gas density, velocity dispersion and temperature distributions and allow one to estimate the star formation efficiency if the stellar mass distribution is known.

The paper is organized as follows. In section 2 we select a model for the stellar mass distribution. In section 3 the conditions for the thermal and mechanical equilibrium are formulated and the equation that determines the residual gas density distribution is derived. We demonstrate then that the velocity dispersion and the star formation efficiency in the post-star-forming cloud follow directly from the equilibrium conditions and the gas density distribution. In section 3.3 we discuss the major sources for the molecular gas heating and cooling and show how to determine the molecular gas temperature. In section 4 we confront our model to the well studied molecular cloud D1 in the nearby dwarf spheroidal galaxy NGC 5253 and show that model predictions are in agreement with several observational characteristics of this cloud and its embedded cluster. Finally, in section 5 we summarize our findings and the major model restrictions.

2. STELLAR MASS DISTRIBUTION

Hereafter it is assumed that star formation in the parental molecular cloud results in a dense compact cluster with a total stellar mass M_{SC} and a Gaussian stellar density distribution:

$$\rho_\star(r) = \frac{M_{SC}}{(2\pi)^{3/2}b^3} \exp\left[-\frac{1}{2}\left(\frac{r}{b}\right)^2\right], \quad (1)$$

$$n_\star(r) = \frac{N_\star}{(2\pi)^{3/2}b^3} \exp\left[-\frac{1}{2}\left(\frac{r}{b}\right)^2\right], \quad (2)$$

where ρ_* is the stellar mass density, N_* and n_* are the total number and the number density of the turbulence-driven stars, respectively. b is the star cluster core radius.

The stellar mass $M_*(r)$ enclosed within a sphere of radius r then is:

$$M_*(r) = M_{SC} \left[\text{erf} \left(\frac{r}{2^{1/2}b} \right) - \left(\frac{2}{\pi} \right)^{1/2} \frac{r}{b} \exp \left[-\frac{1}{2} \left(\frac{r}{b} \right)^2 \right] \right], \quad (3)$$

where $\text{erf}(r)$ is the error function.

3. EQUILIBRIUM CONDITIONS

3.1. Turbulent energy dissipation and regeneration rates

Following [Stone et al. \(1998\)](#); [Mac Low \(1999\)](#); [Basu & Murali \(2001\)](#) we assume that the rate of the turbulent energy dissipation in the residual gas is:

$$Q_{dis}(r) = \frac{\eta_d \rho_g \sigma^3}{\lambda}, \quad (4)$$

where ρ_g and σ are the residual gas density and 1D velocity dispersion, respectively, and λ is the turbulence driving scale. The dimensionless factor $\eta_d \sim 1$ over a range of driving lengths (see [Basu & Murali 2001](#), and references therein). We assume that $\eta_d = 1$ in all our simulations.

In spite of many discussions (e.g. [Basu & Murali 2001](#); [Quillen et al. 2005](#); [Swift & Welch 2008](#); [Brunt et al. 2009](#)) the nature and the value of the driving length remain uncertain. Here we postulate that turbulence in a newborn cluster is supported by massive stars that randomly move in the gravitational well of the cluster. It is likely that in such a case the driving length λ is determined by the separation between neighboring massive stars. The plausible assumption then is that the half of the driving wavelength is equal to the mean distance between the two neighboring massive stars and thus $\lambda = 4X$, where X , the half-distance between neighboring massive stars, is (see [Silich et al. 2020](#)):

$$X(r) = b \left[(9\pi/2)^{1/2} \exp \left[\frac{1}{2} \left(\frac{r}{b} \right)^2 \right] \right]^{1/3} N_*^{-1/3}. \quad (5)$$

Note that in this case the driving length is not constant as it is adopted in most models, but depends on the distance from the star cluster center (the multi-scale energy injection was discussed by [Scalo 1987](#)). This assumption results in the turbulent energy dissipation rate

$$Q_{dis}(r) = \frac{\eta_d \rho_g \sigma^3 N_*^{1/3}}{4(9\pi/2)^{1/6} b \exp \left[\frac{1}{6} \left(\frac{r}{b} \right)^2 \right]}. \quad (6)$$

We assume that the lost turbulent energy is regenerated in the turbulent mixing layers and turbulent wakes formed around most massive stars that move in the gravitational well of the cluster. We further follow arguments presented in [Norman & Silk \(1980\)](#); [McKee \(1989\)](#); [Matzner \(2002\)](#) and assume that recently formed stars support turbulence in the residual gas at the rate

$$Q_*(r) = P \sigma(r) n_*(r) / 2, \quad (7)$$

where P is the average rate of momentum input to the intracloud medium per massive star that includes the momentum input via the stellar wind $\dot{M}_w V_w$, radiation L_*/c and that, due to the photo-heated HII region expansion. The precise value of the momentum continuously returned to the intracloud medium by a typical massive star is uncertain. Here we normalize it to the stellar radiative momentum input rate (see [Henney & Arthur 2019](#)):

$$P = \eta_* L_*/c, \quad (8)$$

where $L_* = L_{bol}/N_*$ is the average turbulence-driving star luminosity, L_{bol} is the star cluster bolometric luminosity and c is the speed of light. The η_* factor is considered as a free parameter of the model. The value of this parameter is determined by the degree to which the feedback energy could be conserved. It depends on the physical conditions in the star-forming cloud, and in general must be determined by numerical simulations. [McKee \(1999\)](#) suggested that $\eta_* \approx 1.6$, to account for the energy stored in the magnetic field, while numerical simulations by [Mackey \(2013\)](#), focused on the dynamics of HII regions around moving O stars, showed that the momentum input rate could exceed

that provided by radiation pressure up to 10 times. It is interesting to note that AGN outflows also often have momentum well in excess (up to 30 times) of the central black hole integrated momentum $L_{BH}\tau_{in}/c$, where τ_{in} is the characteristic time scale of the radiative feedback (see [Faucher-Giguère & Quataert 2012](#), and references therein). We adopt that η_* falls in the range $1 < \eta_* < 10$.

In the dense, compact clusters the characteristic size of individual wind-driven bubbles are much smaller than the cluster core radius b ([Silich & Tenorio-Tagle 2017, 2018](#)). Therefore we assume that the energy dissipation and regeneration rates are balanced locally throughout the cluster: $Q_{dis}(r) = Q_*(r)$. This leads to the relation:

$$\rho_g \sigma^2 = \frac{\eta_*}{\eta_d} \left(\frac{3}{4\pi^4} \right)^{1/3} \frac{L_{bol}}{cb^2 N_*^{1/3}} \exp \left[-\frac{1}{3} \left(\frac{r}{b} \right)^2 \right]. \quad (9)$$

3.2. Mechanical equilibrium

The mechanical equilibrium in the post-star-forming cloud requires the gravitational pull of the cluster to be in balance with the turbulent pressure (e.g. [Calura et al. 2015](#))

$$\frac{dP_{turb}}{dr} = -\frac{G\rho_g(M_g(r) + M_*(r))}{r^2}, \quad (10)$$

where G is the gravitational constant, $M_g(r)$ and $M_*(r)$ are the gas and the stellar mass enclosed within a sphere of radius r , respectively, $P_{turb}(r) = \rho_g \sigma^2$ is the residual gas turbulent pressure.

3.3. Equilibrium gas distribution

Equation (9) allows one to calculate the turbulent pressure derivative: $dP_{turb}/dr = d(\rho_g \sigma^2)/dr$. Combining this derivative with equation (10), one can obtain an equation that determines the residual gas density distribution in a stationary post-star-forming cloud upon the assumption that the turbulent energy dissipation is continuously compensated by the stellar feedback:

$$\begin{aligned} \rho_g(r) &= \frac{\eta_*}{\eta_d} \left(\frac{2}{9\pi} \right)^{1/3} \frac{L_{bol}}{\pi c G b N_*^{1/3} [M_*(r) + M_g(r)]} \left(\frac{r}{b} \right)^3 \exp \left[-\frac{1}{3} \left(\frac{r}{b} \right)^2 \right] \\ &\approx 10^{-14} \frac{\eta_*}{\eta_d} \frac{L_{42}}{N_*^{1/3} b_1 [M_{*,s}(r) + M_{g,s}(r)]} \left(\frac{r}{b} \right)^3 \exp \left[-\frac{1}{3} \left(\frac{r}{b} \right)^2 \right] \text{ g cm}^{-3}, \end{aligned} \quad (11)$$

where $L_{42} = L_{bol}/10^{42} \text{ erg s}^{-1}$, b_1 is the core radius in pc units, $M_{*,s}(r)$ is the stellar and $M_{g,s}(r)$ is the gas mass in solar units. The residual gas mass in equation (11) is:

$$M_g(r) = 4\pi \int_0^r x^2 \rho_g(x) dx. \quad (12)$$

We solve equation (11) by iterations by making use equation (12). At the first step it is assumed that the gas density is equal to zero in the whole star cluster volume. This implies that in equation (11) $M_g(r) = 0$, but allows one to calculate a new, nonzero gas density distribution $\rho_i(r)$ as the stellar density and stellar mass are not equal to zero. A new gas density distribution is used then to integrate equation (12) numerically and obtain a new, nonzero gas mass distribution $M_g(r)$. This $M_g(r)$ is used in equation (11) to improve the gas density distribution. The iteration process continues until the difference between the subsequent values of the integrated gas mass becomes small enough: $| (M_{g,i} - M_{g,i-1}) | / (M_{g,i} + M_{g,i-1}) < \epsilon$. We usually stop iterations when ϵ drops below 10^{-5} . After the residual gas distribution was calculated, one can easily obtain the other characteristics of the star-forming region. The velocity dispersion is calculated by means of equations (9) and (11):

$$\begin{aligned} \sigma(r) &= \left[\frac{3G(M_*(r) + M_g(r))}{2b} \right]^{1/2} \left(\frac{b}{r} \right)^{3/2} \\ &\approx 8 \times 10^{-2} \left[\frac{M_{*,s}(r) + M_{g,s}(r)}{b_1} \right]^{1/2} \left(\frac{b}{r} \right)^{3/2} \text{ km s}^{-1}. \end{aligned} \quad (13)$$

The star formation efficiency is:

$$SFE = M_{SC}/[M_{SC} + M_g(R)], \quad (14)$$

where R is the adopted radius of the cluster. The total turbulent energy dissipation rate in the residual gas is:

$$L_{gas}(R) = 4\pi \int_0^R Q_{dis}(x) x^2 dx. \quad (15)$$

The stellar bolometric and the wind mechanical luminosities do not increase linearly with the stellar mass. We estimate that only (15% - 20%) of massive stars contribute about 90% to the star cluster energy budget and adopt for the number of the turbulence-driven stars

$$N_\star \approx 0.15 \times N_{massive}(M_{SC}/10^6 M_\odot), \quad (16)$$

where $N_{massive}$ is the number of massive ($M > 8 M_\odot$) stars in a $10^6 M_\odot$ cluster. In clusters with a canonical Kroupa IMF $N_{massive} \approx 1.1 \times 10^4$ (e.g. Calura 2015), while in the case of a Salpeter IMF with the lower and upper cutoff masses $3 M_\odot$ and $120 M_\odot$, respectively, $N_{massive} \approx 3.1 \times 10^4$.

3.4. Thermal balance and the molecular gas temperature

The thermal balance in a post-star-forming cloud is determined by the turbulent, cosmic ray and X-ray gas heating and the molecular gas cooling rates (e.g. Maloney et al. 1996; Basu & Murali 2001; Shang et al. 2002; Pan & Padoan 2009; Papadopoulos 2010):

$$Q_{dis} + Q_{CR} + Q_{XR} - Q_{cool} - Q_{gd} = 0. \quad (17)$$

In equation (17) Q_{dis} is the turbulent energy dissipation rate (see equation 4), Q_{CR} and Q_{XR} are the cosmic ray and the X-ray heating rates and Q_{cool} is the molecular gas cooling rate, respectively. Q_{gd} is the energy exchange between the gas and dust grains (see Goldsmith 2001; Pan & Padoan 2009; Papadopoulos 2010):

$$Q_{gd} = 7 \times 10^{-34} n^2 T_g^{1/2} (T_g - T_d) \text{ erg cm}^{-3} \text{ s}^{-1}, \quad (18)$$

where $n = \rho_g/\mu_{mol}$ is the molecular gas number density, μ_{mol} is the mean mass per particle in the molecular gas, T_g and T_d are the molecular gas and the dust grain temperatures. We adopt $\mu_{mol} = 2.33 m_H$, where m_H is the hydrogen atom mass. In the UV-shielded dense environment CR heating rate is determined by the CR ionization rate per H_2 molecule Papadopoulos (2010):

$$Q_{CR} = 1.5 \times 10^{-24} \xi_{CR,17} n_4 \text{ erg cm}^{-3} \text{ s}^{-1}, \quad (19)$$

where $\xi_{CR,17}$ is the CR ionization rate in 10^{-17} s^{-1} and n_4 is the molecular gas number density in the 10^4 cm^{-3} units. The reference value for the ξ_{CR} is $5 \times 10^{-17} \text{ s}^{-1}$ - the average CR ionization rate in our Galaxy. In compact starbursts it may be up to 10^3 times larger Papadopoulos (2010).

The residual molecular gas in dense UV-shielded parcels of the star-forming cloud may be also exposed to and heated by the soft and hard X-ray emission caused by the magnetic lines reconnection in young stellar objects, X-ray binaries or shock-heated stellar winds (e.g. Maloney et al. 1996; Feigelson & Montmerle 1999; Shang et al. 2002; Meijerink & Spaans 2005, and references therein). For example, Tsujimoto et al. (2006) reported the detection of hard X-ray emission from the two UCHIs in W49A, one of the most active star-forming regions in our Galaxy. The X-ray heating rate is given by (Panoglou et al. 2012; Mackey et al. 2019):

$$Q_{XR} = \eta_X n H_X, \quad (20)$$

where η_X is the heating efficiency (see Dalgarno et al. 1999). H_X is the X-ray energy absorption rate per particle (Maloney et al. 1996; Panoglou et al. 2012):

$$H_X = \int_{E_{min}}^{E_{max}} \sigma_X(E) F(E) dE, \quad (21)$$

where $F(E)$ is the X-ray flux and $\sigma_X(E)$ is the photoelectric cross-section per H nucleus.

One can obtain the molecular gas temperature from the energy balance equation (17) by making use a reasonable approximation for the molecular gas cooling rate $Q_{cool} = Q_{cool}(n, T, du/dr)$, where du/dr is the velocity gradient.

4. NGC 5253 CLOUD D1 AND ITS EMBEDDED CLUSTER

In this section we confront our model with NGC 5253 D1 molecular cloud and its young, compact cluster. For the star cluster mass, core radius and metallicity we adopt $M_{SC} = 1.625 \times 10^5 M_\odot$, $b = 0.8$ pc and $Z = 0.2Z_\odot$ (see Turner et al. 2017; Silich et al. 2020). We also adopt a canonical Kroupa initial mass function with lower and upper cutoffs $M_{low} = 0.1 M_\odot$ and $M_{up} = 120 M_\odot$, respectively. In this case $N_\star \approx 270$. We then make use Starburst99 synthetic model to obtain the embedded cluster bolometric luminosity ($L_{bol} = 3.9 \times 10^{42}$ erg s $^{-1}$ at the age of 1 Myr) and calculate the residual gas density distribution. The velocity dispersion is then obtained from equation (13). The stellar mass and the model-predicted gas density distributions are presented by dotted, solid and dashed lines on Fig. 1 panel a, while the velocity dispersion is shown in panel b of this figure. The dotted line on panel a displays the stellar density distribution derived from the Gaussian fit to the radio and infrared (IR) integrated intensity maps (see Turner et al. 2000; Gorjian et al. 2001; Turner et al. 2015, 2017), while the solid and dashed lines present the model-predicted molecular gas distribution for $\eta_\star = 1$ and $\eta_\star = 5$, respectively. The model predicts different stellar and gas density distributions with more extended gas distribution and stellar mass concentrated towards the star cluster center. This is consistent with different core radii in Gaussian fits to the observed IR/radio and molecular gas emissions (Turner et al. 2017).

The corresponding 1D velocity dispersion is shown on panel b. Note that the η_\star value does not affect the velocity

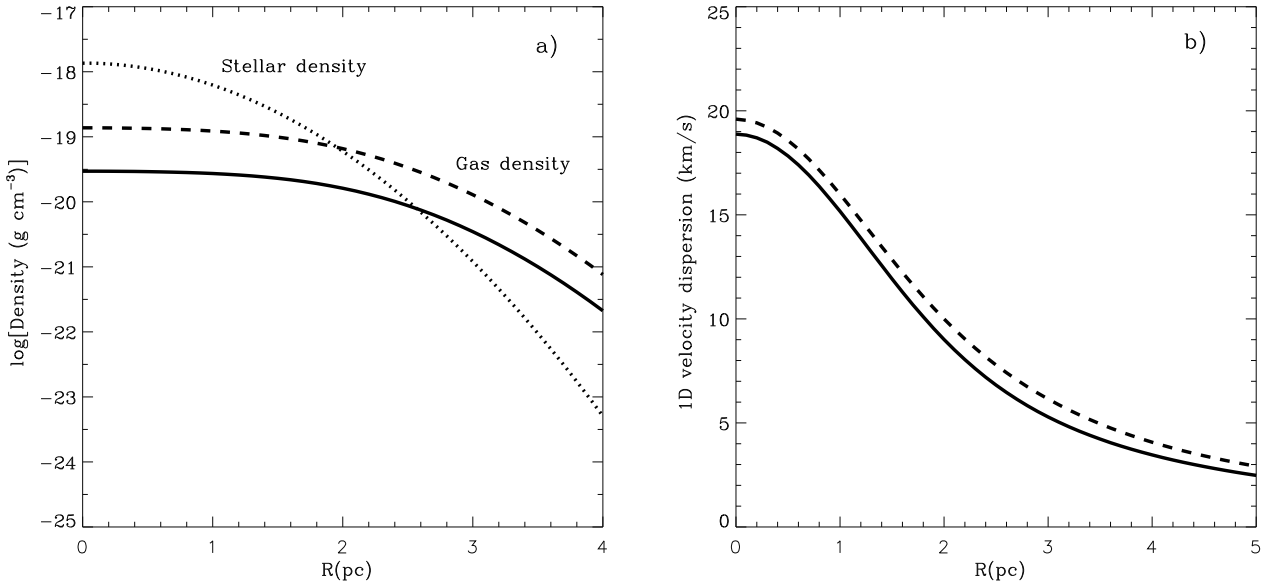


Figure 1. The model-predicted D1 cloud structure. The stellar mass distribution derived from the Gaussian fit to the radio and IR integrated intensity maps is shown by the dotted line in panel a. The solid and dashed lines in this panel display the molecular gas distributions obtained for two different η_\star factor values: $\eta_\star = 1$ (solid line) and $\eta_\star = 5$ (dashed line). The model-predicted velocity dispersion is shown on panel b, where solid and dashed lines correspond to the same models as in panel a.

dispersion significantly as $\sigma \sim 1/\sqrt{\rho} \sim 1/\sqrt{\eta_\star}$ (see equation 13). For distant star-forming regions like NGC 5253 D1 cloud, where the available spatial resolution does not allow to study the velocity dispersion profile, one can make use of the model-predicted velocity dispersion and gas density distributions to calculate the mass-weighted velocity dispersion and compare it with the observed value:

$$\sigma_w = \frac{4\pi}{M_g(R)} \int_0^R \rho_g(x) \sigma(x) x^2 dx. \quad (22)$$

In the case of D1 cloud the mass-weighted velocity dispersion is $\sigma_w \approx 9.3 \text{ km s}^{-1}$ and $\sigma_w \approx 10.4 \text{ km s}^{-1}$ in models with $\eta_\star = 1$ and $\eta_\star = 5$, respectively, that is in good agreement with the observed CO linewidth ($\sigma \approx 9.2 \text{ km s}^{-1}$ Turner et al. 2015, 2017). The molecular gas mass within a 7.5 pc radius in these two cases is $M_g \approx 2.4 \times 10^4 M_\odot$ and $M_g \approx 9.5 \times 10^4 M_\odot$, respectively, which is consistent with the observed CO emission.

In the model-predicted density range the thermal coupling between the dust grains and the molecular gas is weak: Pan & Padoan (2009), see also Appendix E in Whitworth (2016). This implies that the molecular gas temperature could be evaluated from its own energy balance and one can neglect the Q_{gd} term in equations (17) and (24). The turbulent heating rate is about $1.4 \times 10^{37} \text{ erg s}^{-1}$ in the simulations with $\eta_* = 1$ and $7.5 \times 10^{37} \text{ erg s}^{-1}$ when $\eta_* = 5$. In both cases the integrated turbulent heating exceeds the T Tauri integrated X-ray luminosity significantly: $L_{XR,TT} = N_{PMS} \times L_{XTT} \approx 1.2 \times 10^{35} \text{ erg s}^{-1}$, where $N_{PMS} \approx 1.5 \times 10^6 (M_{SC}/10^6 M_\odot)$ is the number of low mass ($M < 3 M_\odot$) pre-main sequence stars and $L_{XTT} \approx 5 \times 10^{29} \text{ erg s}^{-1}$ is a T Tauri star typical luminosity (Shang et al. 2002). Massive stars emit X-rays at a level $\sim 10^{-7} L_{bol}$ (Crowther et al. 2022) that results in a comparable to the T Tauri integrated value: $L_{XR,MS} \approx 10^{-7} L_{bol} = 3.9 \times 10^{35} \text{ erg s}^{-1}$. X-ray emission from the high mass binaries (HMXBs) may reach $(10^{32} - 10^{33}) (M_{SC}/1 M_\odot) \text{ ergs s}^{-1}$ (e.g. Mas-Hesse & Cerviño 1999; Van Bever & Vanbeveren 2000) and thus be comparable or even exceed the turbulent heating rate. However, it takes (4-5) Myr for the HMXBs to become active. The low mass X-ray binaries (LMXBs) become active even at later times. In clusters as young as that in the center of D1 cloud, where the nonthermal radio emission from supernovae was not detected, X-ray heating by binaries is negligible.

The estimates of the X-ray emission from hot cometary-like bubbles formed around massive stars with a strong wind are less certain as depend on the ambient gas density and stellar parameters. The Chandra observations of UCHII regions in Sagittarius B2 (Takagi et al. 2002) and W49A (Tsujiimoto et al. 2006) revealed hard (3.0keV - 8.0keV) X-ray emission within the range $10^{30} \text{ erg s}^{-1}$ - $10^{33} \text{ erg s}^{-1}$, associated with some of the UCHII regions. Numerical modelling of the X-ray emission from the wind-blown bubble around young moving star BD+60°2522 (the Bubble Nebula) led Green et al. (2019) to the similar soft X-ray and 1-2 orders of magnitude smaller hard X-ray luminosities. However, the number of massive stars with strong stellar winds is much (at least two orders of magnitude) smaller than that of T Tauri stars. Therefore it is unlikely that the integrated X-ray heating exceeds the turbulent heating rate unless the intracluster radiation field is dominated by supermassive stars (Smith et al. 2016) or the intracluster gas is exposed to the external sources. Hereafter we neglect gas heating by the X-rays.

The molecular gas cooling rate in this density range could be approximated by the expression (Ao et al. 2013):

$$Q_{cool} = 6 \times 10^{-29} n^{1/2} T_g^3 du/dr \text{ erg cm}^{-3} \text{ s}^{-1}, \quad (23)$$

where du/dr is the rms velocity gradient ($du/dr = \sqrt{3} d\sigma/dr$) in units of $\text{km s}^{-1} \text{ pc}^{-1}$ (see Fig. 2). Note that this approximation must be taken with some care due to uncertainties in the molecular gas composition, molecules depletion onto dust grains, emission lines taken into consideration and their optical depths. If X-ray heating can be neglected and the cooling is dominated by molecular gas whose composition is determined in Table 1 of Goldsmith (2001), the energy balance equation (17) and the approximation to the gas cooling rate (23) yield:

$$T_g = [(Q_{dis} + Q_{CR})/6 \times 10^{-29}]^{1/3} (du/dr)^{-1/3} n^{-1/6} K. \quad (24)$$

The temperature distribution calculated upon the assumption that $\eta_* = 5$ is shown in Fig. 3. Here the solid, dashed and dotted lines present the gas temperatures in the cases when CR ionization rate is equal to that in our Galaxy (see section 3.3), 10 and 100 times larger, respectively. At the Milky Way CR intensity the contribution of the CR heating is negligible. However, at starburst-like ionization rates CR heating becomes significant at the outskirts of the star-forming region as the turbulent heating rate per unit volume drops with radius fast while it is likely that the CR density at the D1 cloud scale remains almost homogeneous because of large diffusion length (e.g. Aharonian et al. 2019). Large predicted molecular gas temperatures are consistent with the large CO(3-2) over CO(2-1) intensity ratio in D1 cloud (see Turner et al. 2015). It is interesting to note that similar large temperature gradients were revealed in a sample of molecular clouds located in the central zone of the Galaxy by Rodríguez-Fernández et al. (2001) and Ao et al. (2013) who also suggested that the dissipation of the supersonic turbulence could be responsible for large molecular gas temperatures.

In the case of D1 cloud the model predicts large star formation efficiencies: $\approx 87\%$ in the case when parameter $\eta_* = 1$ (that is probably not consistent with the assumption of the residual gas retention) and $\approx 63\%$ when $\eta_* = 5$. The last value is in agreement with the large SFE in D1 cloud obtained by Turner et al. (2015), the large SFE ($\sim 47\%$) in ρ Oph cloud (Wilking & Lada 1983) and agrees with the results of numerical simulations by Skinner & Ostriker (2015) who found that SFE may reach 50% - 70% in the case of the large gas opacity to infrared radiation. It is also large enough to this cluster ends up as a gravitationally bound super-star cluster (see Baumgardt & Kroupa 2007; Baumgardt et al. 2008). It is important to note that η_* is not a unique parameter that determines the value of the

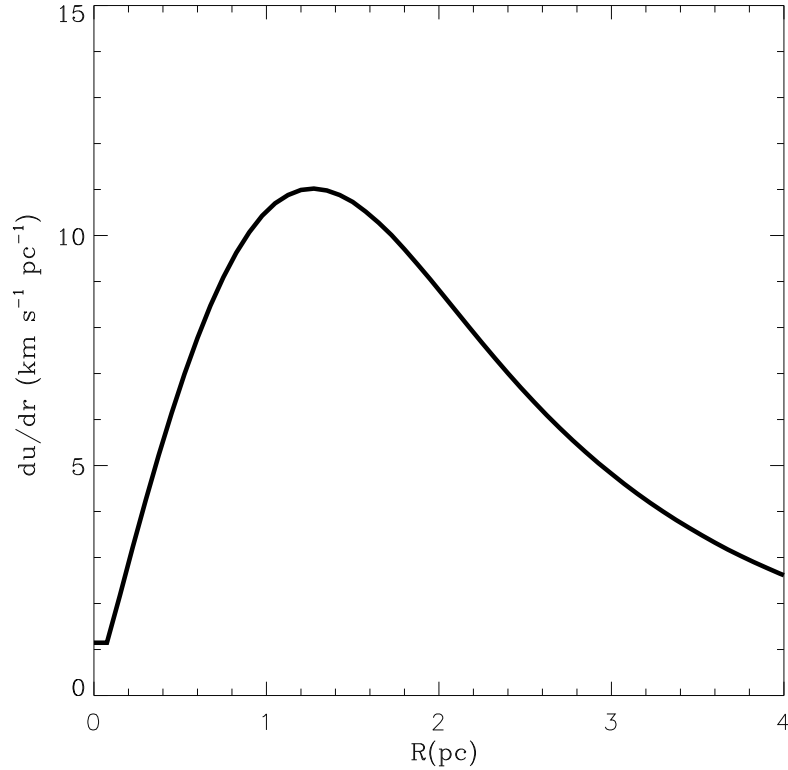


Figure 2. The gas velocity gradient calculated upon the assumption that $\eta_{\star} = 5$.

SFE. Model predictions depend also on the star cluster mass and compactness. For example, the SFE grew to 99% in simulations with $\eta_{\star} = 5$ and core radius $b = 0.1\text{pc}$. It is unlikely that at such large SFE the individual neighboring winds and HII regions do not merge to disperse the parental cloud. We speculate here that it is the star cluster compactness, that leads to a dramatic difference between the deeply embedded into molecular cloud D1 cluster in NGC 5253, and similar in mass and age, but gas-free cluster R136 in the 30 Dor region (Portegies Zwart et al. (2010) and Mackey & Gilmore (2003) estimated the R136 core radius to fall in the range $0.1\text{pc} - 0.3\text{pc}$, see their Tables 3 and 4, respectively). On the other hand, the model-predicted SFE drops rapidly when one considers lower mass clusters. For example, in simulations with $\eta_{\star} = 5$, $M_{SC} = 580 M_{\odot}$ and $b = 0.14\text{pc}$ (parameters similar to the Orion Nebula cluster (ONC), Huff & Stahler 2006), we obtained $\approx 11\%$ efficiency that agrees with the value of the SFE obtained by Huff & Stahler (2006) for ONC and Megeath et al. (2016) for different stellar groups, clusters and clouds in the Orion complex. Certainly, the above examples should be considered only as an illustration because the stellar mass distribution in these clusters differs from the Gaussian one (R136 and ONC were very well fitted by different power-law profiles). In many other cases the star cluster mass distribution is well represented by Moffat, Elson-Fall-Freeman, King and Plummer models (see Portegies Zwart et al. 2010; Cuevas-Otahola et al. 2020; Röser & Schilbach 2019, and references therein). We leave the discussion of different stellar mass distributions to the future communication.

It is instructive to note, that in spite of the large momentum input rate allowed in the simulations (up to $5 \times L_{bol}/c$), the model-predicted turbulence dissipation rate remains negligibly small in comparison with the star cluster bolometric luminosity: $2.2 \times 10^{-5} < L_{dis}/L_{bol} < 1.2 \times 10^{-4}$. This favors the radiative feedback to be the major mechanism that supports turbulence in this cloud, likely through the overpressurised HII regions formed around most massive stars that move in the gravitational well of the cluster (e.g. Mackey et al. 2013; Matzner 2002; Krumholz et al. 2006). Indeed, a low radiative feedback efficiency is expected in dense, dusty environments (see Haid et al. 2018). This agrees with the fact that far infrared (FIR) luminosity of the NGC 5253 central zone ($\approx 8 \times 10^{42} \text{erg s}^{-1}$ Cormier et al. 2015) is comparable and even exceeds the bolometric luminosity of the D1 cluster. In the case of a low feedback efficiency most of the deposited energy is radiated away in the IR regime, instead of being used to unbind the residual gas. Therefore

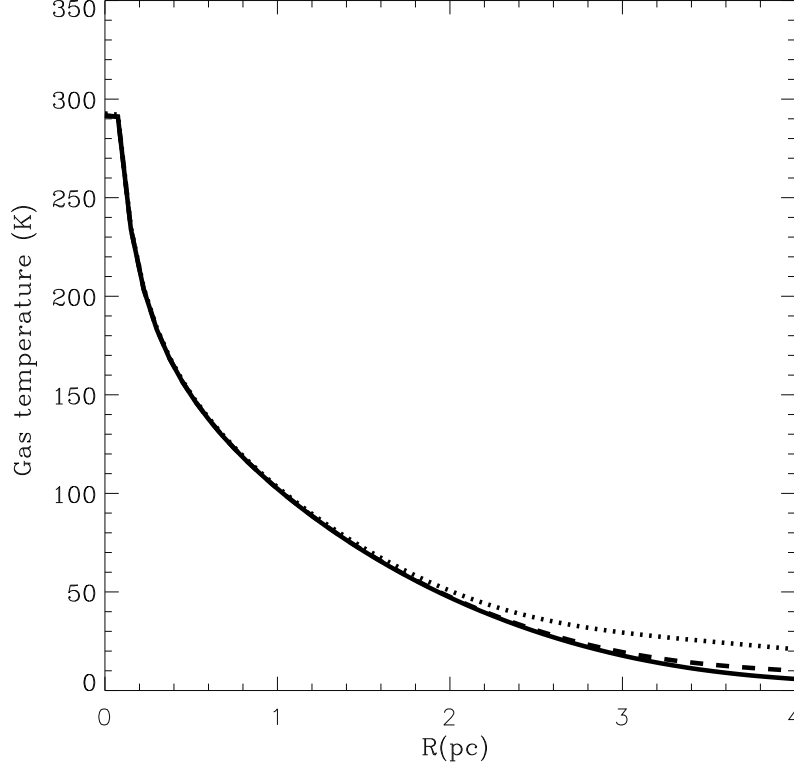


Figure 3. The model-predicted gas temperature distribution. Solid, dashed and dotted lines present the model-predicted temperature distribution in the cases when the CR ionization rate is equal to that in our Galaxy, 10 and 100 times larger, respectively. The temperatures were calculated upon the assumption that $\eta_{\star} = 5$.

one must take care comparing D1 cluster with Fig. 3 from [Baumgardt et al. \(2008\)](#) which confronts the cloud binding to the accumulated radiative energy upon the assumption of a 100% radiative feedback efficiency.

Simulations with a Salpeter IMF with lower and upper cutoff masses $3 M_{\odot}$ and $120 M_{\odot}$ result in slightly larger masses of the residual gas ($\sim 3.9 \times 10^4 M_{\odot}$ and $\sim 1.5 \times 10^5 M_{\odot}$) and smaller star formation efficiencies ($\sim 80\%$ and $\sim 50\%$) in models with $\eta_{\star} = 1$ and $\eta_{\star} = 5$, respectively.

5. CONCLUDING REMARKS

Here we studied the leftover gas density, velocity dispersion and temperature in young stellar clusters with a given stellar mass distribution. It was postulated that star formation in the collapsing cloud is altered via the leftover gas stirring by massive stars which move in the gravitational well of the cluster and the residual gas. It was also assumed that the cluster is sufficiently compact and dense to prevent the leftover gas expulsion, and that the post-star-forming system is stable. The last condition requires the gradient of the turbulent pressure to be in balance with the gravitational pull of the cluster and the rapidly dissipated turbulent energy to be regenerated continuously. The last condition requires a sufficient number of massive stars to be formed. Therefore the steady-state condition determines both, the residual gas properties, and the star formation efficiency in clusters with a suppressed star cluster wind.

We confront this model with properties of a compact cluster in a nearby dwarf spheroidal galaxy NGC 5253 that is still deeply obscured by molecular cloud D1. The model is in good agreement with several observed properties of this cluster in spite that infalling molecular filaments still supply gas to the central zone of the galaxy ([Consiglio et al. 2017](#)). It predicts the different stellar and gas density distributions with stellar mass more concentrated towards the star cluster center. The model-predicted mass-weighted velocity dispersion is in good agreement with the observed value, while high molecular gas temperatures are consistent with the large observed CO(3-2) over CO(2-1) intensity ratio. The large predicted star formation efficiency is sufficient for this cluster to end up as a bound super star cluster.

The model suggests that turbulent energy dissipation may be an effective energy source for the molecular gas heating in dense and compact strongly obscured clusters as was also suggested by [Pan & Padoan \(2009\)](#). It is likely that turbulent heating results in molecular gas warm component that could be detected in Far Infrared (FIR) low-excitation emission lines of oxygen, carbon and other species and also in millimeter/submillimeter CO rotational lines, while gas in Photon Dominated Regions (PDRs), directly heated by Far Ultraviolet (FUV) and X-ray photons, is manifested by the FIR high-excitation lines. CO and FIR emission lines in NGC 5253 were detected by ALMA (see [Turner et al. 2017](#)) and Herschel ([Cormier et al. 2015](#)). The observed [OI]63 μ m and [OI]145 μ m lines luminosity is about $6.1 \times 10^{39} \text{ erg s}^{-1}$ at the distance of about 4Mpc, that is larger than the model-predicted turbulent energy dissipation rate. However the Herschel observations do not separate D1 from other sources. The CO(3-2) line luminosity is smaller, about $8.8 \times 10^{35} \text{ erg s}^{-1}$. James Webb Space Telescope(JWST) sensitivity and subarcsecond space resolution are required to reveal the contribution of D1 cloud to the observed infrared emission. It is also crucial to obtain better restrictions on the total CO luminosity and on the temperature of warm molecular gas by observing higher J CO lines.

The fraction of the stellar feedback used to regenerate the turbulent energy dissipation rate is not fixed in the present model and will be addressed in a forthcoming communication. Nevertheless, the value of the momentum input rate used in the simulations is motivated by the numerical simulations and requires that only a tiny fraction of the radiation energy be used to compensate the turbulent energy dissipation rate.

One can apply this model to clusters with an arbitrary mass distribution, but must note that it is restricted to massive and compact clusters with a suppressed mechanical feedback. It is likely, however, that our model could be also applied to lower mass, less compact and massive, very compact clusters with an extremely large SFE prior to their residual gas dispersal if their parental clouds are supported against gravity by the turbulent pressure and contract gradually in the quasi-static regime, as was suggested by [Huff & Stahler \(2006\)](#) for the Orion Nebula cluster.

Certainly, the equilibrium conditions that we have used should change after the onset of the supernova explosions. The further evolution of leftover gas is beyond the scope of the present paper. We anticipate two possible scenarios: the leftover gas could be expelled out of the cluster by supernovae, that, however, is unlikely in systems with a sharp density gradient (see [Jiménez et al. 2021](#)), or the turbulent energy dissipates after the majority of massive stars explode as supernovae and the leftover gas, enriched by massive star products, collapses to form a second stellar generation.

ACKNOWLEDGEMENTS

We thank our anonymous referee for his/her constructive comments and S. Beck for careful reading of the manuscript. This study was supported by CONACYT, México research grant A1-S-28458. JLT acknowledges the support of U.S. National Science Foundation grant AST2006433. JM acknowledges support from a Royal Society-Science Foundation Ireland University Research Fellowship and S.M.G. acknowledges the support provided by CONACYT through Cátedra n.482.

REFERENCES

- | | |
|---|--|
| Aharonian, F., Yang, R., & de Oña Wilhelmi, E. 2019, <i>Nature Astronomy</i> , 3, 561 | Consiglio, S. M., Turner, J. L., Beck, S., et al. 2017, <i>ApJ</i> , 850, 54 |
| Ao, Y., Henkel, C., Menten, K. M., et al. 2013, <i>A&A</i> , 550, A135 | Cormier, D., Madden, S. C., Lebouteiller, V., et al. 2015, <i>A&A</i> , 578, A53 |
| Arthur, S. J., & Hoare, M. G. 2006, <i>ApJS</i> , 165, 283 | Crowther, P. A., Broos, P. S., Townsley, L. K., et al. 2022, <i>MNRAS</i> , 515, 4130 |
| Basu, S., & Murali, C. 2001, <i>ApJ</i> , 551, 743 | Cuevas-Otahola, B., Mayya, Y. D., Puerari, I., & Rosa-González, D. 2020, <i>MNRAS</i> , 492, 993 |
| Baumgardt, H., & Kroupa, P. 2007, <i>MNRAS</i> , 380, 1589 | Dalgarno, A., Yan, M., & Liu, W. 1999, <i>ApJS</i> , 125, 237 |
| Baumgardt, H., Kroupa, P., & Parmentier, G. 2008, <i>MNRAS</i> , 384, 1231 | Elmegreen, B. G., & Scalo, J. 2004, <i>ARA&A</i> , 42, 211 |
| Binette, L., Flores-Fajardo, N., Raga, A. C., Drissen, L., & Morisset, C. 2009, <i>ApJ</i> , 695, 552 | Faucher-Giguère, C.-A., & Quataert, E. 2012, <i>MNRAS</i> , 425, 605 |
| Brunt, C. M., Heyer, M. H., & Mac Low, M. M. 2009, <i>A&A</i> , 504, 883 | Feigelson, E. D., & Montmerle, T. 1999, <i>ARA&A</i> , 37, 363 |
| Calura, F., Few, C. G., Romano, D., & D’Ercole, A. 2015, <i>ApJ Let</i> , 814, L14 | Franco, J., Shore, S. N., & Tenorio-Tagle, G. 1994, <i>ApJ</i> , 436, 795 |

- Goldsmith, P. F. 2001, *ApJ*, 557, 736
- Gorjian, V., Turner, J. L., & Beck, S. C. 2001, *ApJ Let*, 554, L29
- Green, S., Mackey, J., Haworth, T. J., Gvaramadze, V. V., & Duffy, P. 2019, *A&A*, 625, A4
- Haid, S., Walch, S., Seifried, D., et al. 2018, *MNRAS*, 478, 4799
- Henney, W. J., & Arthur, S. J. 2019, *MNRAS*, 486, 3423
- Huff, E. M., & Stahler, S. W. 2006, *ApJ*, 644, 355
- Jiménez, S., Tenorio-Tagle, G., & Silich, S. 2021, *MNRAS*, 505, 4669
- Krumholz, M. R., Matzner, C. D., & McKee, C. F. 2006, *ApJ*, 653, 361
- Krumholz, M. R., & McKee, C. F. 2005, *ApJ*, 630, 250
- Mac Low, M.-M. 1999, *ApJ*, 524, 169
- Mac Low, M.-M., & Klessen, R. S. 2004, *Reviews of Modern Physics*, 76, 125
- Mackey, A. D., & Gilmore, G. F. 2003, *MNRAS*, 338, 85
- Mackey, J., Gvaramadze, V. V., Mohamed, S., & Langer, N. 2015, *A&A*, 573, A10
- Mackey, J., Langer, N., & Gvaramadze, V. V. 2013, *MNRAS*, 436, 859
- Mackey, J., Walch, S., Seifried, D., et al. 2019, *MNRAS*, 486, 1094
- Maloney, P. R., Hollenbach, D. J., & Tielens, A. G. G. M. 1996, *ApJ*, 466, 561
- Marks, M., & Kroupa, P. 2012, *A&A*, 543, A8
- Mas-Hesse, J. M., & Cerviño, M. 1999, in *Wolf-Rayet Phenomena in Massive Stars and Starburst Galaxies*, ed. K. A. van der Hucht, G. Koenigsberger, & P. R. J. Eenens, Vol. 193, 550
- Matzner, C. D. 2002, *ApJ*, 566, 302
- McKee, C. F. 1989, *ApJ*, 345, 782
- McKee, C. F. 1999, in *NATO Advanced Study Institute (ASI) Series C*, Vol. 540, *The Origin of Stars and Planetary Systems*, ed. C. J. Lada & N. D. Kylafis, 29
- McKee, C. F., & Ostriker, E. C. 2007, *ARA&A*, 45, 565
- Megeath, S. T., Gutermuth, R., Muzerolle, J., et al. 2016, *AJ*, 151, 5
- Meijerink, R., & Spaans, M. 2005, *A&A*, 436, 397
- Melnick, J., Moles, M., Terlevich, R., & Garcia-Pelayo, J.-M. 1987, *MNRAS*, 226, 849
- Murray, N., Quataert, E., & Thompson, T. A. 2010, *ApJ*, 709, 191
- Norman, C., & Silk, J. 1980, *ApJ*, 238, 158
- Padoan, P. 1995, *MNRAS*, 277, 377
- Padoan, P., Federrath, C., Chabrier, G., et al. 2014, in *Protostars and Planets VI*, ed. H. Beuther, R. S. Klessen, C. P. Dullemond, & T. Henning, 77
- Padoan, P., & Nordlund, Å. 2011, *ApJ*, 730, 40
- Pan, L., & Padoan, P. 2009, *ApJ*, 692, 594
- Panoglou, D., Cabrit, S., Pineau Des Forêts, G., et al. 2012, *A&A*, 538, A2
- Papadopoulos, P. P. 2010, *ApJ*, 720, 226
- Portegies Zwart, S. F., McMillan, S. L. W., & Gieles, M. 2010, *ARA&A*, 48, 431
- Quillen, A. C., Thorndike, S. L., Cunningham, A., et al. 2005, *ApJ*, 632, 941
- Rodríguez-Fernández, N. J., Martín-Pintado, J., Fuente, A., et al. 2001, *A&A*, 365, 174
- Röser, S., & Schilbach, E. 2019, *A&A*, 627, A4
- Scalo, J. M. 1987, in *Interstellar Processes*, ed. D. J. Hollenbach & J. Thronson, Harley A., Vol. 134, 349
- Shang, H., Glassgold, A. E., Shu, F. H., & Lizano, S. 2002, *ApJ*, 564, 853
- Shu, F. H., Adams, F. C., & Lizano, S. 1987, *ARA&A*, 25, 23
- Silich, S., & Tenorio-Tagle, G. 2017, *MNRAS*, 465, 1375
- Silich, S., & Tenorio-Tagle, G. 2018, *MNRAS*, 478, 5112
- Silich, S., Tenorio-Tagle, G., Martínez-González, S., & Turner, J. 2020, *MNRAS*, 494, 97
- Skinner, M. A., & Ostriker, E. C. 2015, *ApJ*, 809, 187
- Smith, L. J., Crowther, P. A., Calzetti, D., & Sidoli, F. 2016, *ApJ*, 823, 38
- Solomon, P. M., Rivolo, A. R., Barrett, J., & Yahil, A. 1987, *ApJ*, 319, 730
- Stone, J. M., Ostriker, E. C., & Gammie, C. F. 1998, *ApJ Let*, 508, L99
- Swift, J. J., & Welch, W. J. 2008, *ApJS*, 174, 202
- Takagi, S.-i., Murakami, H., & Koyama, K. 2002, *ApJ*, 573, 275
- Tenorio-Tagle, G., Munoz-Tunon, C., & Cox, D. P. 1993, *ApJ*, 418, 767
- Terlevich, R., & Melnick, J. 1981, *MNRAS*, 195, 839
- Tsujimoto, M., Hosokawa, T., Feigelson, E. D., Getman, K. V., & Broos, P. S. 2006, *ApJ*, 653, 409
- Turner, J. L., Beck, S. C., Benford, D. J., et al. 2015, *Nature*, 519, 331
- Turner, J. L., Beck, S. C., & Ho, P. T. P. 2000, *ApJ Let*, 532, L109
- Turner, J. L., Consiglio, S. M., Beck, S. C., et al. 2017, *ApJ*, 846, 73
- Van Bever, J., & Vanbeveren, D. 2000, *A&A*, 358, 462
- Vazquez-Semadeni, E., Ostriker, E. C., Passot, T., Gammie, C. F., & Stone, J. M. 2000, in *Protostars and Planets IV*, ed. V. Mannings, A. P. Boss, & S. S. Russell, 3
- Wareing, C. J., Zijlstra, A. A., & O'Brien, T. J. 2007, *ApJ Let*, 660, L129
- Whitworth, A. P. 2016, *MNRAS*, 458, 1815
- Wilkings, B. A., & Lada, C. J. 1983, *ApJ*, 274, 698

Williams, J. P., & McKee, C. F. 1997, ApJ, 476, 166

Wirth, H., Kroupa, P., Haas, J., et al. 2022, MNRAS, 516,
3342